chemosensors

MDPI

Article

Thiourea Organocatalysts as Emerging Chiral Pollutants: En Route to Porphyrin-Based (Chir)Optical Sensing

Nele Konrad [1], Matvey Horetski [1,2], Mariliis Sihtmäe [3], Khai-Nghi Truong [4], Irina Osadchuk [1,5], Tatsiana Burankova [6], Marc Kielmann [7], Jasper Adamson [3], Anne Kahru [3], Kari Rissanen [4], Mathias O. Senge [7], Victor Borovkov [1,*], Riina Aav [1,*] and Dzmitry Kananovich [1,*]

1 Department of Chemistry and Biotechnology, School of Science, Tallinn University of Technology, Akadeemia tee 15, 12618 Tallinn, Estonia; nele.konrad@taltech.ee (N.K.); matvey.horetski@gmail.com (M.H.); irina.osadchuk@taltech.ee (I.O.)
2 Department of Polymer Chemistry, Belarusian State University, Leningradskaya 14, 220050 Minsk, Belarus
3 National Institute of Chemical Physics and Biophysics, Akadeemia tee 23, 12618 Tallinn, Estonia; mariliis.sihtmae@kbfi.ee (M.S.); jasper.adamson@kbfi.ee (J.A.); anne.kahru@kbfi.ee (A.K.)
4 Department of Chemistry, University of Jyvaskyla, P.O. Box 35, Survontie 9B, 40014 Jyväskylä, Finland; khai-nghi.kn.truong@jyu.fi (K.-N.T.); kari.t.rissanen@jyu.fi (K.R.)
5 ICGM, University Montpellier, CNRS, ENSCM, 34000 Montpellier, France
6 Process Analytics, Hamilton Bonaduz AG, Via Crusch 8, 7402 Bonaduz, Switzerland; tburankova@yahoo.de
7 School of Chemistry, Trinity Biomedical Sciences Institute, Trinity College Dublin, The University of Dublin, Dublin, Ireland; kielmanm@tcd.ie (M.K.); sengem@tcd.ie (M.O.S.)
* Correspondence: victor.borovkov@taltech.ee (V.B.); riina.aav@taltech.ee (R.A.); dzmitry.kananovich@taltech.ee (D.K.)

check for updates

Citation: Konrad, N.; Horetski, M.; Sihtmäe, M.; Truong, K.-N.; Osadchuk, I.; Burankova, T.; Kielmann, M.; Adamson, J.; Kahru, A.; Rissanen, K.; et al. Thiourea Organocatalysts as Emerging Chiral Pollutants: En Route to Porphyrin-Based (Chir)Optical Sensing. *Chemosensors* **2021**, *9*, 278. https://doi.org/10.3390/chemosensors9100278

Academic Editor: Bolze Frederic

Received: 31 August 2021
Accepted: 24 September 2021
Published: 29 September 2021

Abstract: Environmental pollution with chiral organic compounds is an emerging problem requiring innovative sensing methods. Amino-functionalized thioureas, such as 2-(dimethylamino)cyclohexyl-(3,5-bis(trifluoromethyl)phenyl)thiourea (Takemoto's catalyst), are widely used organocatalysts with virtually unknown environmental safety data. Ecotoxicity studies based on the *Vibrio fischeri* luminescence inhibition test reveal significant toxicity of Takemoto's catalyst (EC_{50} = 7.9 mg/L) and its NH_2-substituted analog (EC_{50} = 7.2–7.4 mg/L). The observed toxic effect was pronounced by the influence of the trifluoromethyl moiety. En route to the porphyrin-based chemosensing of Takemoto-type thioureas, their supramolecular binding to a series of zinc porphyrins was studied with UV-Vis and circular dichroism (CD) spectroscopy, computational analysis and single crystal X-ray diffraction. The association constant values generally increased with the increasing electron-withdrawing properties of the porphyrins and electron-donating ability of the thioureas, a result of the predominant Zn···N cation–dipole (Lewis acid–base) interaction. The binding event induced a CD signal in the Soret band region of the porphyrin hosts—a crucial property for chirality sensing of Takemoto-type thioureas.

Keywords: porphyrin; thiourea; chiral amine; organocatalyst; Takemoto's catalyst; host–guest binding; chirality; supramolecular chemistry; circular dichroism; toxicity; chiral pollutants; *Vibrio fischeri*

1. Introduction

The production of chiral chemicals is rapidly growing to satisfy the continuously increasing demand in various industrial and medicinal fields. Enantiomerically pure compounds often show improved bioactivity, fewer adverse effects, and increased selectivity over their achiral or racemic counterparts. More than 50% of pharmaceuticals and around 30% of pesticides are chiral, and their numbers are steadily growing [1–3]. An adverse effect of this process has increased the amount of pollution caused by chiral chemicals, representing a potential threat for ecosystems [4–7]. However, noteworthy ecotoxicology data are frequently unavailable and the environmental fate remains unclear for numerous artificial

chiral compounds. The alarming increase in pollution calls for the development of innovative sensing methods to detect chiral pollutants in the natural environment [8,9]. Notably, a holistic approach for their detection should comprise both chemoselectivity and chirality sensing since opposite enantiomers may have different ecotoxicity, accumulation, and biodegradation rates. It turns out that the application of supramolecular chemistry [10–12], which relies on the formation of host–guest complexes between a sensor (host) and an analyte (guest), is an appealing direction to develop effective sensory systems. In this regard, porphyrins represent a family of unique sensing materials, which can effectively detect nonchiral and chiral analytes upon deposition onto a solid-state support [13,14]. In case of chiral analytes, simultaneous chirality sensing is possible due to chirality transfer phenomena (also designated as supramolecular chirogenesis) [15]. The binding event, most commonly occurring via coordination of a specific functional group in a chiral analyte to a metal ion in the porphyrin, produces a noticeable (chir)optical response in circular dichroism (CD) spectra. The produced CD signal can usually be correlated with the chirality of the guest, based on the well-defined structure of the host–guest complex [16–19]. Although this approach has been frequently applied to determine the absolute configuration of various chiral organic compounds, the design of porphyrin-based sensors for chemoselective detection of a specific chiral pollutant remains a challenging task.

As a rule, chiral pollutants are structurally diverse organic compounds containing multiple functional groups, which could potentially act as competitive binding sites and be involved in various non-covalent interactions. Such diversity could result in poorly interpretable net (chir)optical outcomes due to the generation of multiple structurally different host–guest assemblies upon interaction with a porphyrin host. The effects of various functional groups in a polyfunctionalized analyte on its (chir)optical response have not been investigated in detail and represent an arduous task in view of the tremendous structural diversity. Fortunately, the most common structural features can be outlined in the majority of typical chiral pollutants to simplify the problem. (1) Nitrogen-containing molecules are prevalent among pharmaceuticals and agrochemicals [20–22], and basic nitrogen moieties are therefore able to serve as privileged binding sites to zinc porphyrin-based sensors due to strong Zn···N cation–dipole interaction [23–25]. (2) Additional functional groups, which can act as a secondary binding site or participate in other non-covalent interactions (such as hydrogen bonding), are also common [26–28], along with (3) aromatic rings decorated with electron-donating/withdrawing substituents. While factor (1) is well-studied, we assume that the impact of (2) and (3) on the key Zn···N binding event could be revealed by performing a systematic study with a series of structurally similar model compounds to "mimic" the organization of typical polyfunctionalized chiral pollutant. For this purpose, we selected a family of chiral analytes comprising 2-aminocyclohexyl arylthioureas **1a–d** (Figure 1b). This was to perform binding studies with a series of zinc porphyrin hosts (Figure 1a), to assess the influence of additional functional groups and electronic effects, and to reveal the most suitable host–guest combinations exhibiting the strongest (chir)optical responses for reliable solution-phase detection by UV-Vis and CD spectroscopy. Additional information was derived from crystal structure determination and DFT calculations.

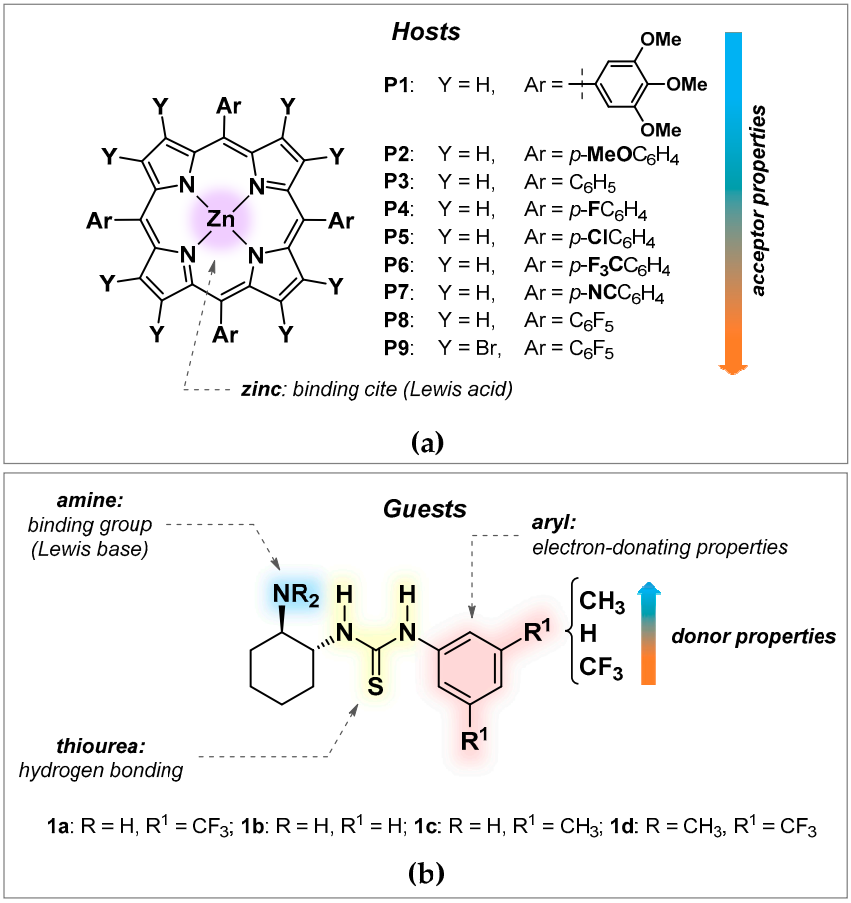

Figure 1. (**a**) Structures of zinc porphyrins **P1**–**P9** used as hosts and detector entities for plausible chemosensors; (**b**) Scope of chiral 2-aminocyclohexyl arylthioureas **1a**–**d** (depicted as *R*,*R*-enantiomers), studied in this work as guest molecules and model pollutants with highlighting the diversity of binding sites.

Another motivation to test the (chir)optical detection of compounds **1a–d** as model analytes is due to their widespread use as chiral organocatalysts. Enantioselective organocatalysis is believed to be a sustainable and world-changing chemical innovation, which has been highlighted by IUPAC as one of the "top ten emerging technologies in chemistry" in 2019 [29]. Since the pivotal discoveries of Schreiner [30], Jakobsen [31], and Takemoto [32], thioureas have found widespread use as prominent hydrogen-bonding organocatalysts [32–34]. They are used to prepare diverse chiral materials [33,35,36], including stereoselective ring-opening polymerization for the production of biodegradable polymers [37–39]. According to the SciFinder database [40], the parent Takemoto's catalyst **1d** has been mentioned in 406 documents, including 44 patents, emphasizing its prominence also for commercial applications. In general, the thiourea catalysts are often referred to as a safer and sustainable alternative to the transition metal catalysts, in particular, because of the overstated toxicity of transition metal compounds [41,42]. However, the evidence for the environmental safety of organocatalysts is currently scarce [43]. The cytotoxic effect was recently revealed for a 3,5-bis(trifluoromethyl)phenyl thiourea derivative [44] that raised a reasonable concern about its potential harm. Here we report the results of an ecotoxicological evaluation of thioureas **1a–d**, based on the *Vibrio fischeri* (also known as *Aliivibrio fischeri*) bioluminescence inhibition test [45].

2. Materials and Methods

General methods. UV-Vis absorption spectra were recorded on a Jasco V-730 double-beam spectrophotometer (JASCO International Co., Ltd., Tokyo, Japan) in a 1 cm thermally

stabilized screw-cap quartz cuvette with a septum cap. CD spectra were recorded on a Jasco J-1500 spectrophotometer (JASCO International Co., Ltd., Tokyo, Japan) in a 1 cm screw cap quartz cuvette in analytical grade CH_2Cl_2 at 293 K. The data acquisition was performed in the 375–475 nm range with the scanning rate of 50 nm/min, bandwidth of 2.6 nm, response time of 4 s, and accumulations in three scans. ^{1}H NMR spectra were recorded in $CDCl_3$ at 293 K, using a QCI CryoProbe on a Bruker AVANCE III 800 MHz spectrometer (Bruker Corporation, Billerica, MA, USA). The number of scans was in the range of 8 to 64 scans and was optimized for the samples to obtain a signal to noise ratio of 250 in the recorded spectra. A relaxation delay of 5 s was used. The acquisition time was set to 2.4 s. The spectra were processed in MestReNova 14.2 software and zero filled to 128k points to obtain chemical shifts for finding the dimerization constants. The chemical shifts (δ) were reported in ppm and referenced to a $CHCl_3$ residual peak at 7.26 ppm.

Materials. (1*R*,2*R*)-2-aminocyclohexyl thioureas (*R*,*R*)-**1a–c** were prepared by the known method [46,47] from (1*R*,2*R*)-1,2-diaminocyclohexane and corresponding aryl isothiocyanates. Corresponding (1*S*,2*S*)-enantiomer of (*S*,*S*)-**1a** was prepared from (1*S*,2*S*)-1,2-diaminocyclohexane. The purity and identity of the synthesized compounds **1a–c** were confirmed by ^{1}H and ^{13}C NMR spectroscopy and their NMR spectral data were in agreement with the previously reported values [47]. A sample of (1*S*,2*S*)-thiourea (*S*,*S*)-**1d** (Takemoto's catalyst) was purchased from Strem Chemicals. Stereochemistry labels were used only in CD section.

Porphyrins **P1**–**P8**, except for **P3**, were prepared by insertion of zinc ion into the corresponding free base porphyrins by following the standard experimental protocol [48,49]. Starting free base porphyrins and zinc(II) tetraphenylporphyrin (ZnTPP, **P3**) were purchased from PorphyChem. Porphyrin **P9** was prepared as previously described [50]. The purity and chemical identity of the prepared Zn porphyrins was validated by NMR and UV-Vis spectroscopy.

Spectroscopic Titrations. All the solutions were prepared and mixed by using properly calibrated analytic glassware (Hamilton® Gastight syringes, volumetric flasks, Reno, Nevada, USA). All weights were balanced with a Radwag MYA 11.4 microbalance (accuracy $\pm$ 6 µg). The concentration of zinc porphyrin was held constant throughout the titration sequence. The titration data were fitted by using the online software Bindfit [51–53]. The UV-Vis spectrophotometric titration experiments were performed in analytical grade CH_2Cl_2. To a solution of zinc porphyrin, a solution of guest (dissolved in a stock solution of the host to keep the concentration of the host constant) was added portion-wise using a gastight syringe at 293 K. The corresponding changes in bathochromic shift of the Soret band were monitored at different concentrations of the guest.

Self-association of thioureas **1a** and **1c** has been studied by measuring changes in the chemical shifts of diagnostic protons in the ^{1}H NMR spectra upon dilution [54,55]. To determine the dimerization constants, the experimental data were fitted using the numpy (1.18.5) and scipy (1.4.1) libraries of Python 3 (see the Supplementary Materials for details).

Single crystal X-ray analysis. Crystals of the (*R*,*R*)-**1b**·**P5** complex were obtained by slow solvent evaporation from an equimolar mixture of (*R*,*R*)-**1b** and **P5** (0.005 mmol of each), dissolved in dichloromethane/methanol (v:v, 2:1, 1.5 mL). The single-crystal X-ray data of complex (*R*,*R*)-**1b**·**P5** were acquired using a dual-source Rigaku SuperNova diffractometer equipped with an Atlas detector and an Oxford Cryostream cooling system using mirror-monochromated Cu-K_α radiation (λ = 1.54184 Å). Data collection and reduction for all complexes were performed using the program CrysAlisPro [56] and the Gaussian face-index absorption correction method was applied [56]. The structures were solved with Direct Methods (SHELXS) [57–59] and refined by full-matrix least-squares based on F^2 using SHELXL-2015 [57–59]. Non-hydrogen atoms were assigned anisotropic displacement parameters unless stated otherwise. The hydrogen atoms bonded to nitrogens were located from Fourier difference maps and refined with an N−H distance restraint of approximately 0.96 Å. Other hydrogen atoms were placed in idealized positions and included as riding. The isotropic displacement parameters for all H atoms were constrained to multiples of the

equivalent displacement parameters of their parent atoms with U_{iso}(H) = 1.2 U_{eq}(parent atom). A few reflections with large discrepancies between the calculated and observed structure factors have been omitted from the least-squares refinement as outliers. The X-ray single crystal data and experimental details as well as CCDC number are given below.

Crystal data for the 1:1 complex of (*R*,*R*)-**1b** and **P5**: CCDC 2081478, $C_{58}H_{45}Cl_6N_7SZn$, M = 1150.14 g mol^{-1}, purple rod, 0.14 × 0.04 × 0.03 mm^3, monoclinic, space group $P2_1$ (No. 4), a = 11.7790(2) Å, b = 17.1139(7) Å, c = 13.1976(4) Å, α = 90°, β = 95.215(2)°, γ = 90°, V = 2649.42(14) Å^3, Z = 2, D_{calc} = 1.442 gcm^{-3}, F(000) = 1180, μ = 4.164 mm^{-1}, T = 120(2) K, θ_{max} = 76.42 °, 27314 total reflections, 8639 with $I_o > 2\sigma(I_o)$, R_{int} = 0.0497, 9519 data, 658 parameters, 1 restraints, GooF = 1.029, R_1 = 0.0408 and wR_2 = 0.0925 [$I_o > 2\sigma(I_o)$], R_1 = 0.0472 and wR_2 = 0.0957 (all reflections), 0.387 < dΔρ < −0.477 eÅ^{-3}, Flack parameter x = 0.007(12).

Computational details. A set of previously found conformers for the **1a**·**P3** complex [60] was modified according to the substitution pattern of a new host–guest complex **1a**·**P6** and optimized using RI approximation [61–63], PB86 functional [64,65], D3 dispersion correction [66], def2-SV(P) basis set [67], and Turbomole 7.0 software [68]. The method showed a good agreement with the experimental data [69–71]. To confirm that the geometry corresponds to energy minima, the frequency calculations were done on the same level of theory. To include solvent effects, single point calculations were performed using the RI-BP86-D3/def2-TZVP [72] level of theory and COSMO continuum solvent model [73] with ε = 8.93 for CH_2Cl_2. The corresponding geometries and energies are provided in the Supplementary Materials. The quantum theory of atoms in molecule (QTAIM) [74,75] calculations by AIMAll Version 19.10.12 [76] and Natural bond orbital (NBO) [77,78] analysis by v 3.1 software [79], which is embedded within Gaussian 16 software [80], were performed to confirm the presence of noncovalent interactions. QTAIM calculations were done using the RI-BP86-D3/def2-SV(P) level of theory and for NBO calculations the ωB97XD [81]/cc-pVDZ [82–84] level of theory and SMD (CH_2Cl_2) [85] were used. The geometries were visualized by GaussView 6 [86].

Toxicity Evaluation. Acute bioluminescence inhibition assay (exposure time 30 min) with naturally bioluminescent bacteria *Vibrio fischeri* was performed at ambient temperature (~293 K) on white sterile 96-well polypropylene microplates (Greiner Bio-One GmbH, Frickenhausen, Germany) following the Flash assay protocol (ISO, 2010) [87]. The bacterial suspension used for the toxicity measurements was prepared from freeze-dried bacteria originating from a *Vibrio fischeri* reagent (Aboatox, Turku, Finland). As amino-functionalized thioureas are poorly soluble in water their stock solutions were prepared in methanol (final concentration of MeOH in the toxicity test was 1.5% that is a not toxic concentration to *Vibrio fischeri*) and then 2% NaCl was added. The highest tested concentration for the test chemicals was 50 mg/L, except for Takemoto's catalyst for which it was 6.45 mg/L. Briefly, 100 μL of the test solution in 3% MeOH and 2% NaCl was pipetted into each well, which was supplemented with 100 μL of bacterial suspension in 2% NaCl by automatic dispensing in a Microplate Luminometer Orion II (Berthold Detection Systems, Pforzheim, Germany) testing chamber. All the chemicals were tested on three different days, in 5–7 dilutions in two replicates for each chemical. The controls, both negative (1.5% MeOH in 2% NaCl) and positive ($ZnSO_4$, prepared from $ZnSO_4 \cdot 7H_2O$), were included in each run. The inhibition of bacterial bioluminescence by the tested compounds was calculated as a percentage of the unaffected control (1.5% MeOH in 2% NaCl) after 30 min contact time. Inhibition of bacterial luminescence (INH%) by the analyzed compounds was calculated as follows:

$$\mathrm{INH\%} = 100 - \frac{\mathrm{IT_{30}} \cdot 100}{\mathrm{KF} \cdot \mathrm{IT_0}} \cdot 100 \quad (1)$$

with

$$\mathrm{F} = \frac{\mathrm{IC_{30}}}{\mathrm{IC_0}} \quad (2)$$

where KF (correction factor) characterizes the natural loss of bioluminescence of the control (i.e., bacterial suspension in 1.5% MeOH in 2% NaCl). IC_0 and IT_0 are the maximum values of bioluminescence during the first 5 s after dispensing 100 µL of test bacteria to 100 µL of control and test sample, respectively. IC_{30} and IT_{30} are the respective bioluminescence values after 30 min. The toxicity values (30-min EC_{50}, which is the concentration of a compound reducing the bioluminescence by 50% after contact time of 30 min) and their confidence intervals were determined from dose–response curves based on the nominal exposure concentrations using the log-normal model of MS Excel macro Regtox [88].

3. Results and Discussion

3.1. Toxicity Studies

In the current study, amino-functionalized thioureas (**1a–d**, Figure 1b) were screened for toxicity using a *Vibrio fischeri* 30-min kinetic luminescent bacteria test according to the Flash-test protocol (see above). *Vibrio fischeri* is a naturally bioluminescent marine bacterium, thus being an environmentally relevant test organism. Moreover, these bacteria are important ecosystem members as biodegraders. The *Vibrio fischeri* bioluminescence inhibition assay is a rapid, cost-efficient, and sensitive analytical tool, which has been widely used for toxicity testing of different types of chemicals [89,90] and polluted environmental samples (such as wastewaters and sediments) [91]. Importantly, this bioassay data have widely been used for the quantitative structure–activity relationship (QSAR) models analysis to predict the toxicity of organic chemicals by their chemical structures [92]. The decrease in bacterial luminescence results from the chemical's adverse effects on the bacterial membrane and consequently their energy metabolism and occurs after brief contact with toxicants (ranging from seconds to minutes depending on the compounds) [93].

The experimentally determined 30-min EC_{50} values of *Vibrio fischeri* for amino-functionalized thioureas are presented in Table 1. Based on the simplified hazard classification scheme described in [92] the studied chemicals can be ranked according to the respective 30-min EC_{50} values as follows: $\leq$1 mg/L = very toxic; >1–10 mg/L = toxic; >10–100 mg/L = harmful; >100 mg/L = "not classified / not harmful". As a result, Takemoto's catalyst (*S*,*S*)-**1d** and its NH_2-substituted siblings ((*R*,*R*)- and (*S*,*S*)-**1a**) were found to be ranked as toxic analogously to the used positive control ($ZnSO_4$). At the same time, phenyl- and 3,5-dimethylphenyl thioureas ((*R*,*R*)-**1b** and **1c**) showed no inhibitory properties up to the maximum concentration tested (EC_{50} > 50 mg/L). It is of note that no significant difference in the EC_{50} values was observed for both (*R*,*R*)- and (*S*,*S*)-enantiomers of **1a**. All tested compounds with the CF_3-group had a similar slope in their dose–response curve (Figure 2), indicating a similar mechanism of the toxic action.

Table 1. Toxicity (30-min EC_{50}, mg/L) of amino-functionalized thioureas **1a–d** and the used positive control ($ZnSO_4$) to *Vibrio fischeri* [a].

Thiourea	*Vibrio fischeri*		
	30-min EC_{50}, mg/L	**95% Confidence Interval**	
(*R*,*R*)-**1a**	7.4	6.5	7.5
(*S*,*S*)-**1a**	7.2	6.2	7.2
(*R*,*R*)-**1b**	>50 [b]	–	–
(*R*,*R*)-**1c**	>50 [b]	–	–
(*S*,*S*)-**1d**	7.9	6.8	9.3
$ZnSO_4$ (as Zn^{2+})	4.2	4.0	4.6

[a] The EC_{50} values are calculated from the dose–response curves presented in Figure 2. [b] The highest concentration tested.

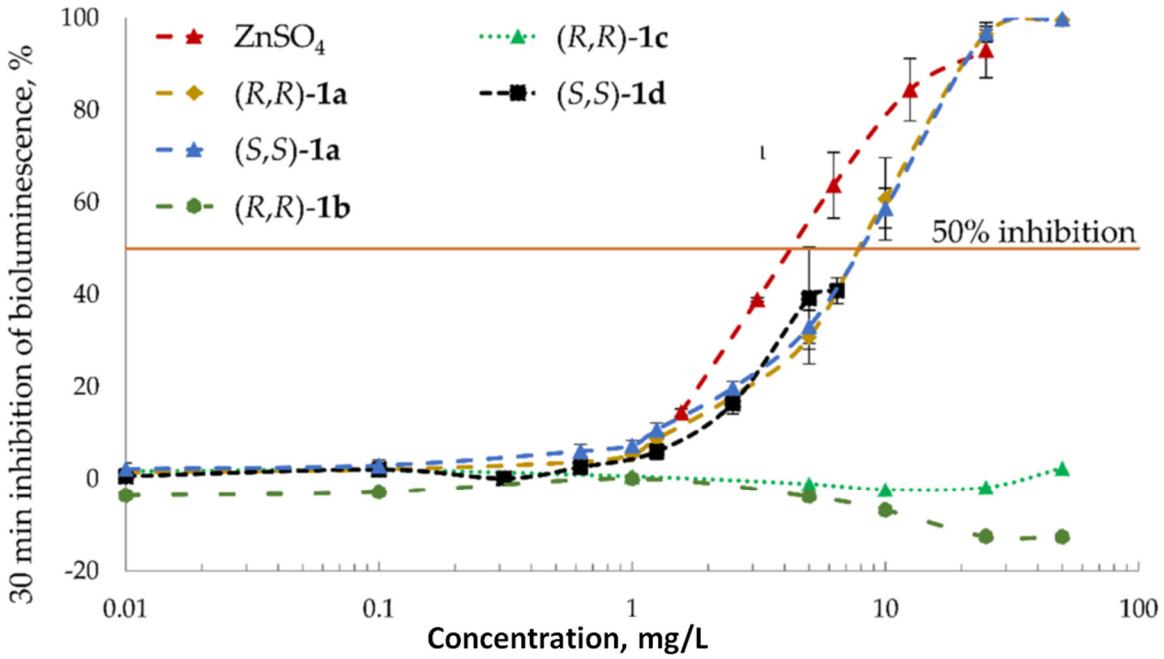

Figure 2. The dose–effect curves of tested amino-functionalized thioureas towards bacteria *Vibrio fischeri*. The respective EC_{50} values are presented in Table 1. Note the logarithmic scale of *x*-axis.

The toxic effect of thioureas **1a** and **1d** evidently arises from the 3,5-bis(trifluoromethyl) phenyl group [94]. Importantly, the same moiety is crucial to enhance the organocatalytic activity and selectivity of thiourea catalysts [95–97]. The ecotoxicity studies presented above, along with steadily expanding applications of thiourea catalysts, highlight their status as plausible emerging chiral pollutants, for which detection methods in solution have yet to be developed.

3.2. Binding and Structural Studies

Complexation of **1a–d** with zinc porphyrins **P1**–**P9** is a reversible process that occurs *via* coordination of the amino group in **1a–d** to zinc ion in a porphyrin host (Figure 3a). This produces a measurable spectral change for the detection of amino-functionalized thioureas **1a–d** in solution. This complexation can conveniently be followed by conventional UV-Vis spectroscopy and results in corresponding bathochromic shifts of the porphyrin Soret and Q bands with the representative example of **1a**·**P5** complex shown in Figure 3b (see the Supplementary Materials for other host–guest systems).

The structures of the complexes formed are most reliably identified and described by crystallography and DFT geometry calculations, respectively. The crystallographic data for **1b**·**P5** complex provides proof for the 1:1 complex formation via coordination of the amino group in **1b** to the zinc ion of porphyrin **P5** (Figure 4). The guest thiourea is resting in a favorable *syn-anti* conformation with respect to the N–H orientation in the thiourea moiety [98]. One of the N–H bonds in the NH_2 group is stabilized by the sulfur atom of **1b** with a N···S distance of 3.266 Å and a contact angle of 160.6° leading to a short intermolecular N–H···S hydrogen bond. The phenyl ring in **1b** is tilted out of plane of the thiourea unit with a torsional angle $\varphi(C_{(=S)}–N–C_{Ph}–C_{Ph}) = 86.1°$. It is nearly perpendicular to the porphyrin plane and parallel to the neighboring aryl substituent in the porphyrin host, albeit the distance between the rings' centroids (~6 Å) is too high for any π–π or π–σ interactions between the aromatic moieties of the host and the guest to be involved [99].

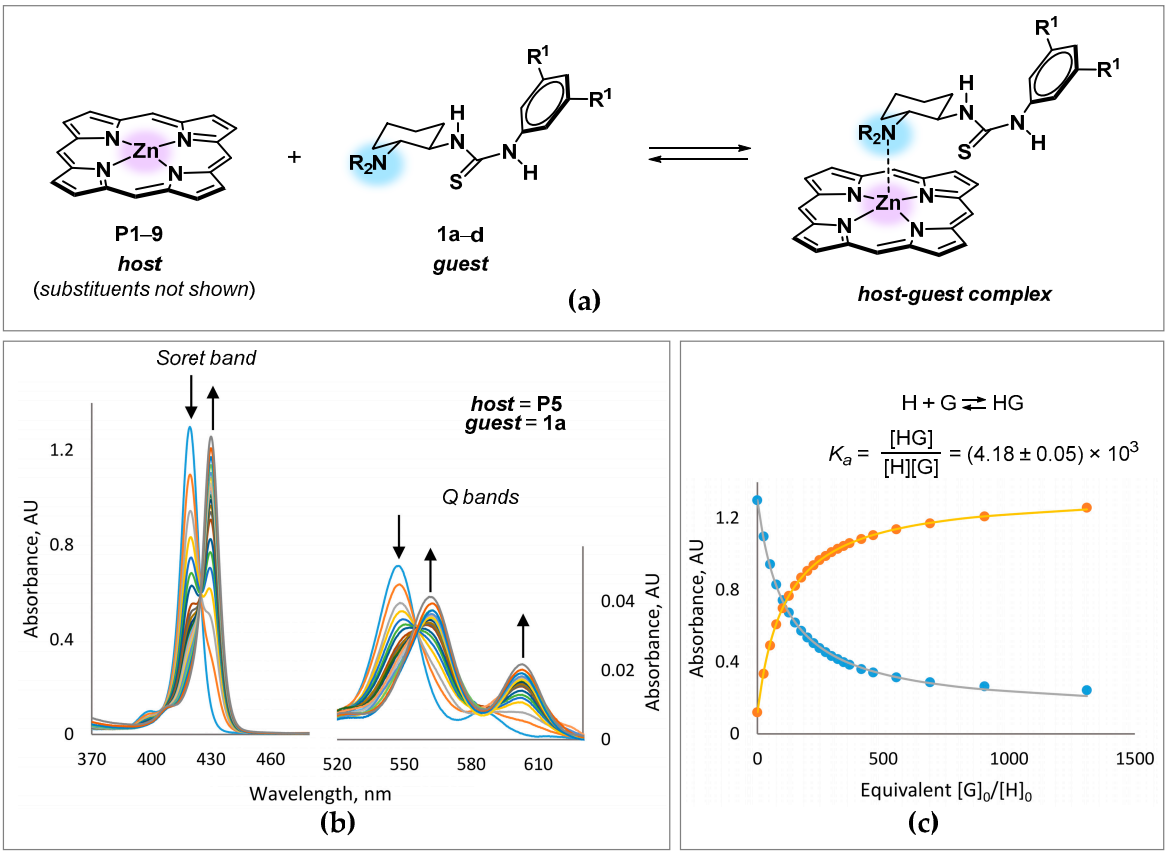

Figure 3. (**a**) Schematic representation of the complexation process of zinc porphyrins (substituents not shown) with 2-aminocyclohexyl arylthioureas; (**b**) representative UV-Vis spectroscopic titration (measured in CH_2Cl_2) of **P5** with **1a**: addition of **1a** (0–2.8 × 10^{-3} M) causes bathochromic shifts of the porphyrin Soret band and Q bands (enlarged, 3×); (**c**) representative 1:1 binding isotherm for the same **P5**-**1a** host–guest system. The complete datasets for all studied host–guest pairs are provided in the Supplementary Material.

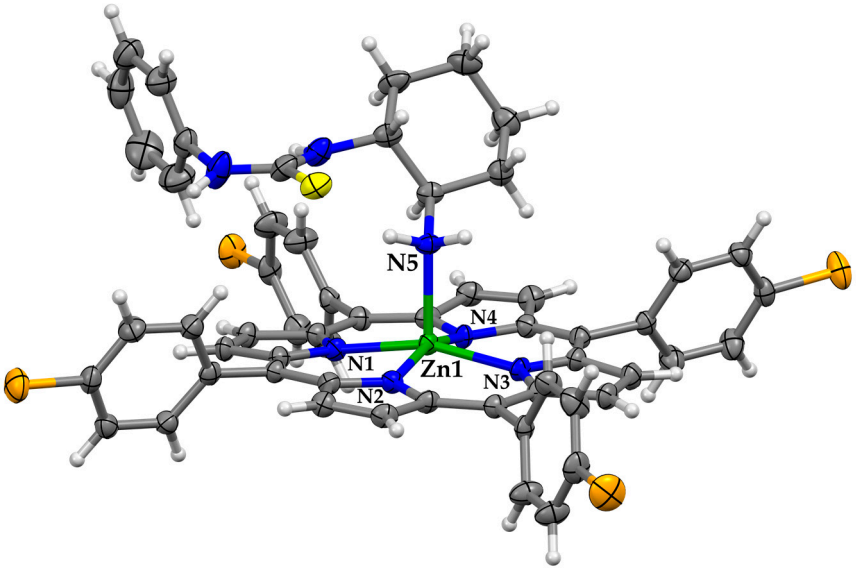

Figure 4. Displacement ellipsoid plot of the (*R*,*R*)-**1b**·**P5** complex. Displacement ellipsoids are drawn at the 50% probability level. The co-crystallized CH_2Cl_2 molecule has been omitted for clarity. Selected interatomic distances (Å): Zn1···N1 2.075(4), Zn1···N2 2.080(4), Zn1···N3 2.070(3), Zn1···N4 2.075(4), Zn1···N5 2.131(3).

Typically for zinc porphyrin complexes, the zinc ion is penta-coordinated and slightly displaced out of the mean porphyrin plane towards the nitrogen atom of the NH_2 group, with a Zn···N distance of 2.131 Å. Coordination of the chiral guest **1b** induces an asymmetric distortion of the porphyrin plane. Consequently, it resulted in reducing the symmetry for the D_{4h}-symmetric porphyrin core to a C_1 point group, which was confirmed using the normal–coordinate structural decomposition method (NSD) [100,101] via the NSD online tool [102] (see the Supplementary Materials for details).

Although the solid-state structure explicitly confirmed the 1:1 complex formation, the analysis of spectroscopic titration data raised some concerns regarding the alleged involvement of more complex stoichiometry in solution [52]. For example, the titration curve for **P5-1a** host–guest system can be successfully fitted with either 1:1 or 1:2 binding isotherms (see the Supplementary Materials, Figures S14 and S15, Table S5). While the former yielded a K_a value of 4180 ± 50 (with SSR error 2.8×10^{-3}), using the 1:2 isotherm gave stepwise association constants: K_1 = 3940 ± 20 and K_2 = 50 ± 10 (with SSR error 8.0×10^{-4}). The K_1 value remained close to this obtained with the 1:1 model and could be attributed to the dominant Zn···N interaction, while the small K_2 association constants could be related to weak binding of the second thiourea guest through hydrogen bonding. This is not surprising, taking into account the well-known self-aggregating behavior of thioureas in solution [54,103–106]. Indeed, measuring the concentration dependence of chemical shifts in ^{1}H NMR for diagnostic NH protons of **1a** and **1c**, revealed weak self-association in solution, with the values of dimerization constants of around 2.9 and 3.4 M^{-1}, for **1a** and **1c** respectively (see the Supplementary Material). However, the values of the chemical shifts remained virtually unchanged in the typical UV-Vis titration concentration range (10^{-4}–10^{-2} M). Based on these results, we neglected the presence of [host]·[guest]$_2$ species and used the 1:1 fitting model to provide valid association constants suitable for comparative analysis.

The obtained K_a values and absorption maxima in the UV-Vis spectra for all 25 host–guest complexes studied are summarized in Table 2. The knowledge of association constants is essential to select the porphyrin host producing the most significant analytical response in terms of sensitivity and selectivity. In addition, it provides a useful insight into the binding mechanism and nature of the supramolecular interactions involved, which are necessary prerequisites in the rational design of an efficient chemical sensor.

We have shown previously that the complexation of **1a-c** with ZnTPP (**P3**) occurs predominantly via the amino nitrogen atom, while the thiocarbonyl group has a low binding affinity to the zinc ion in **P3** [60]. Also, the values of association constants increased with rising the electron-donating ability of corresponding guests (**1a** < **1b** < **1c**) and the electron-withdrawing properties of the hosts (zinc(II) tetraphenylporphyrin > zinc(II) octaethylporphyrin), hence clearly indicating a predominantly electrostatic (Lewis acid-base) nature of the host–guest interaction. Since the association constant for coordination of **1a** to ZnTPP (**P3**) did not exceed 2300 M^{-1}, we supposed that further increasing the electron-withdrawing properties of a porphyrin host could lead to even greater values of the association constants, and therefore to enhanced sensitivity of the guest's detection in solution. This trend can be explicitly revealed by measuring the corresponding association constants for a series of substituted ZnTPPs **P1**–**P9** with steady elevation of the electron-deficiency at the zinc cation (Figure 1b).

As expected, both **1b** and **1c** showed a gradual increase in the association constants with rising the electron-withdrawing properties of the hosts (Table 2, lines 10–14 and 15–22, respectively). Within these series, as expected, the largest association constant of (1.41 ± 0.04) × 10^5 was determined for a combination of the most electron-donating guest **1c** and the highly electron-deficient C_6F_5-substituted porphyrin **P8** (Table 2, line 22). For *p*-substituted ZnTPPs **P2**–**P7**, the trend can be conveniently visualized by using a Hammett plot (Figure 5), showing a clear linear dependence of the logK_a values on the Hammett σ_{para} substituents constants in zinc porphyrins **P2**–**P7**. Surprisingly, thiourea **1a** violated the observed rule upon coordinating to the *p*-CF_3 (**P6**), and *p*-CN (**P7**) substituted

porphyrins (Table 2, lines 6 and 7). Considerably lower association constants were observed in these two particular cases compared to the extrapolation based on the Hammett plot (Figure 5, black line). It is of note that the attenuation was even more substantial in the case of the more electron-deficient *p*-CN substituted porphyrin host **P7** than *p*-CF_3 porphyrin **P6**.

Table 2. Association constants (K_a), Hammett substituent constants (σ_{para}) for *para* substituted benzene rings in porphyrins **P2**–**P7**, and absorption maxima (λ_{max}) in UV-Vis spectra for complexes of thioureas **1a**–**d** with zinc porphyrins **P1**–**P9** measured in CH_2Cl_2.

Entry	Complex	σ_{para} [a]	λ_{max}, nm (log ε)	K_a, M^{-1} (in CH_2Cl_2 at 293K) [b]
1	**1a**·**P1**	–	433 (5.78), 563 (4.34), 604 (4.07)	$(9.0 \pm 0.1) \times 10^2$
2	**1a**·**P2**	−0.27	432 (5.72), 566 (4.21), 610 (4.19)	$(2.05 \pm 0.01) \times 10^3$
3	**1a**·**P3**	0.00	429 (5.77), 563 (4.26), 603 (4.03) [c]	$(2.30 \pm 0.04) \times 10^3$
4	**1a**·**P4**	0.06	429 (5.63), 562 (4.13), 602 (3.85)	$(3.39 \pm 0.07) \times 10^3$
5	**1a**·**P5**	0.23	430 (5.77), 561 (4.28), 603 (4.00)	$(4.18 \pm 0.05) \times 10^3$
6	**1a**·**P6**	0.54	429 (5.78), 562 (4.31), 602 (3.94)	$(2.13 \pm 0.02) \times 10^3$
7	**1a**·**P7**	0.66	432 (5.65), 564 (4.23), 605 (3.92)	$(1.42 \pm 0.02) \times 10^3$
8	**1a**·**P8**	–	425 (5.70), 556 (4.35), 602 (3.04)	$(1.27 \pm 0.02) \times 10^4$
9	**1a**·**P9**	–	470 (5.28), 604 (4.11)	$(5.2 \pm 0.6) \times 10^5$
10	**1b**·**P2**	−0.27	432 (5.65), 565 (4.14), 608 (4.06)	$(5.8 \pm 0.3) \times 10^3$
11	**1b**·**P3**	0.00	429 (5.74), 563 (4.23), 603 (3.98) [c]	$(7.640 \pm 0.003) \times 10^3$
12	**1b**·**P5**	0.23	430 (5.80), 563 (4.32), 603 (4.05)	$(9.8 \pm 0.1) \times 10^3$
13	**1b**·**P6**	0.54	429 (5.08), 563 (4.31), 602 (3.94)	$(1.413 \pm 0.007) \times 10^4$
14	**1b**·**P7**	0.66	432 (5.66), 564 (4.25), 604 (3.93)	$(1.91 \pm 0.02) \times 10^4$
15	**1c**·**P1**	–	433 (5.76), 564 (4.30), 605 (4.02)	$(8.2 \pm 0.5) \times 10^3$
16	**1c**·**P2**	−0.27	432 (5.72), 566 (4.20), 607 (4.13)	$(8.35 \pm 0.03) \times 10^3$
17	**1c**·**P3**	0.00	429 (5.77), 563 (4.26), 603 (4.02) [c]	$(1.116 \pm 0.006) \times 10^4$
18	**1c**·**P4**	0.06	430 (5.71), 562 (4.20), 603 (3.95)	$(1.221 \pm 0.005) \times 10^4$
19	**1c**·**P5**	0.23	430 (5.78), 564 (4.29), 604 (4.02)	$(1.24 \pm 0.01) \times 10^4$
20	**1c**·**P6**	0.54	429 (5.75), 562 (4.28), 602 (3.89)	$(2.16 \pm 0.01) \times 10^4$
21	**1c**·**P7**	0.66	433 (5.63), 565 (4.21), 605 (3.91)	$(2.66 \pm 0.03) \times 10^4$
22	**1c**·**P8**	–	425 (5.69), 556 (4.34)	$(1.41 \pm 0.04) \times 10^5$
23	**1d**·**P3**	0.00	no strong complex formed	n.d. [d]
24	**1d**·**P8**	–	425 (5.53), 556 (4.27)	$(4.5 \pm 0.1) \times 10^2$
25	**1d**·**P9**	–	472 (5.22), 606 (4.10)	$(1.16 \pm 0.07) \times 10^4$

[a] Hammett substituent constant is taken from [107]. [b] Errors are fitted for the 1:1 binding isotherm. [c] The host–guest system has been previously described [60]. [d] The association constant is too low for the UV-Vis spectroscopic titration measurement (n.d. = not determined).

The outliers are evidently due to the presence of strong electron-withdrawing groups (CF_3 and CN) in the aryl rings of both the hosts **P7**, **P6**, and the guest **1a**, which should introduce a noticeable perturbation of the host–guest complex geometry and result in a considerable decrease in the corresponding association constants. Indeed, the DFT calculations showed a different geometry for the main conformer of **1a**·**P6** in comparison with the previously studied complex **1a**·**P3** **[60]** and significant overall change in the conformational composition of these two complexes. Thus, in the complex **1a**·**P3**, the two most populated conformers (abundance 48.6% and 24.5% at 298 K) have a similar face-to-face orientation of one aryl of host **P3** and another aryl of guest **1a** [60] (Figure 6). On the contrary, a T-shaped orientation of aryl substituents was observed in two main conformers of **1a**·**P6** (abundance 46.6% and 37.9% at 298 K) (see Figure 6 and Table S28 in the Supplementary Materials). The differences in geometries and conformational composition also result in elongation of the Zn–N_{guest} bond in **1a**·**P6** compared to **1a**·**P3** (weighted-average values 2.155 Å and 2.145 Å, respectively; see Table S29 in the Supplementary Materials). This explains the weaker binding for the **1a**·**P6** complex (Table 2, entries 3 and 6).

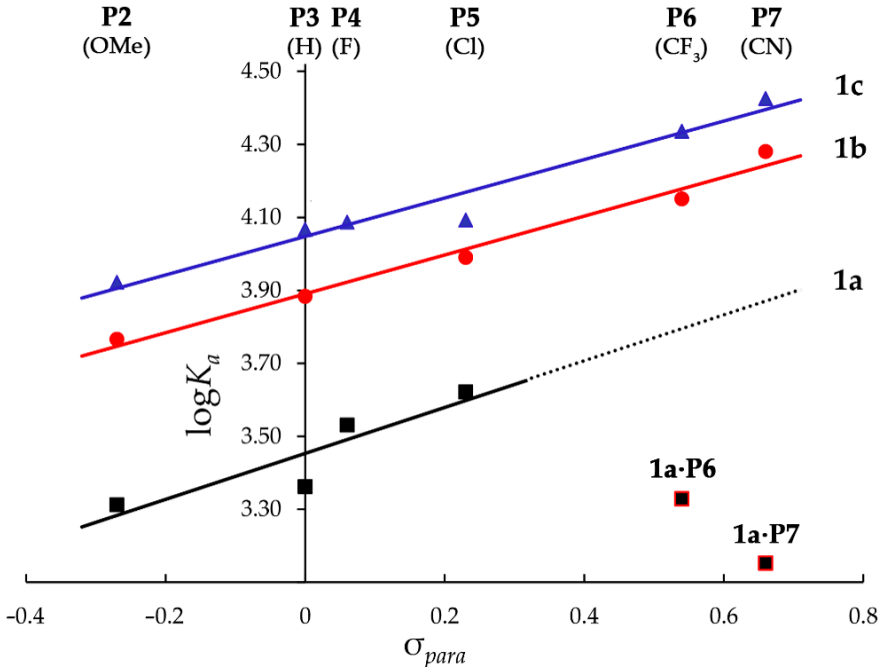

Figure 5. Hammett plots of logK_a vs. σ_{para} constants for coordination of **1a** (black points, outliers are marked with red rim), **1b** (red points), and **1c** (blue points) to zinc tetraphenylporphyrins **P2**–**P7** with *para* substituents in the benzene rings.

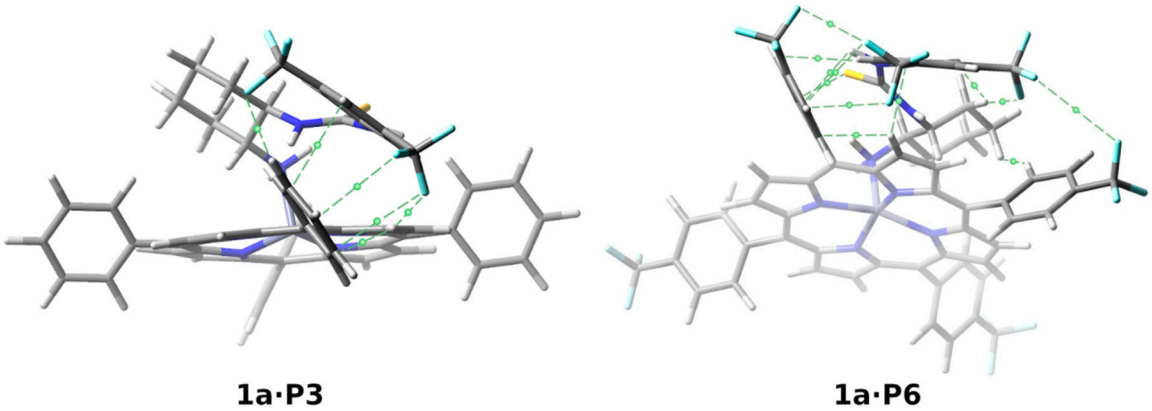

Figure 6. Models for the dominant conformers of complex **1a**·**P3** (**left**) with face-to-face and complex **1a**·**P6** (**right**) with T-shaped orientation of aryls from host–guest. Color code for atoms: C, gray; H, white; N, blue; S, yellow; F, light-blue.

The topological analysis of electron density in the complex **1a**·**P3** with the aid of the quantum theory of atoms in molecule (QTAIM) approach reveals many non-covalent interactions between the host and the guest. Despite a short distance, ca 3.8 Å between centroids [60] of the close-by phenyls of the guest **1a** and host **P3**, and the presence of a C···C bond path between the aryl carbon atoms belonging to the different rings, the electron density at the bond critical point is 0.008 a.u. (see Figure 6 and Table S30 in the Supplementary Materials). Such low electron density is characteristic of a weak and unstable π–π interaction in **1a**·**P3**. [108,109]. The QTAIM approach also reveals the presence of weak interactions between H···C, H···F, and F···C atoms in the aryls of the host–guest pair. Natural bond orbital (NBO) analysis confirmed the presence of weak stabilizing effects of the interactions between the same H···C, H···F, and F···C atoms with the estimated second-order stabilization energies of 2.90 kcal mol^{-1}, and, from the π–π stacking, the second-order stabilization energy was 7.78 kcal mol^{-1} for **1a**·**P3** complex (Figure 6 and

Table S32 in the Supplementary Materials) [110]. The Zn···N second-order stabilization energies were 143.64 kcal mol^{-1} (Table S32 in the Supplementary Materials).

In the main conformers of complex **1a**·**P6**, the CF_3 groups in the host **P6**, and the guest **1a** force the aryl substituents to adopt a T-shaped orientation (see Figure 6 and Table S31 in the Supplementary Materials). This agrees with the previous theoretical study where it was shown that an electronegative substituent makes the T-shaped orientation of aryls more favorable due to the exchange or dispersion of the component's contribution to the binding energy [111]. Here, the NBO partial charges are very similar on the host and guest aryls in both complexes (see Table S31 in the Supplementary Materials). The QTAIM approach proves the presence of σ/π interactions by the electron density at the bond critical point $\rho(r)$ = 0.008 a.u. and the Laplacian of electron density, showing alternation in electronic charge, is positive. These characteristics are typical for such interactions [112].

Moreover, a weak dispersion and strong non-covalent interactions between the H···C, H···F, F···C, and S···H atoms provided additional stabilization of **1a**·**P6**. The NBO analysis showed that the T-shaped orientation of aryls resulted in smaller values of the second-order stabilization energies from π–π stacking (1.90 kcal mol^{-1}), compared to those of complex **1a**·**P3** (7.78 kcal mol^{-1}). On the other hand, the non-covalent interactions between the H···C, H···F, F···C, and S···H atoms additionally stabilized the complex **1a**·**P6** by 7.58 kcal mol^{-1}. In contrast, in the **1a**·**P3** complex this energy was only 2.9 kcal mol^{-1} (see Table S32 in the Supplementary Materials). The Zn···N second-order stabilization energies were 139.08 kcal mol^{-1}, that is, 4.56 kcal mol^{-1} smaller compared to complex **1a**·**P3** (see Table S32 in the Supplementary Materials). However, the overall stabilizing effect was about 5.76 kcal mol^{-1} smaller than that of the complex **1a**·**P3**. Therefore, we can conclude that the cumulative effect of the different conformational composition and additional interactions were responsible for the observed attenuation of the binding strength of host–guest pairs with electron-withdrawing groups on the aryls.

However, the observed attenuation of binding of **1a** to electron-deficient **P6** and **P7** could be surpassed with even more electron-deficient porphyrin hosts, such as **P8** and **P9** (Table 2), by increasing the strength of the dominant Zn···N interaction. Indeed, porphyrins **P8** and **P9** resulted in remarkably high association constants of (1.27 ± 0.02) × 10^4 and (5.2 ± 0.6) × 10^5, respectively (Table 2 lines 8 and 9). Similar to the **1c**·**P8** system, the case of **1a**·**P9** represented another extreme K_a value, a consequence of the electron-withdrawing character and the non-planar saddle distortion [113–115] of **P9**, which additionally enhanced the binding of the axial ligands [49].

Replacing the NH_2 group in **1a** with the NMe_2 group in Takemoto's catalyst **1d** weakened the binding strength considerably due to a sterically less accessible nitrogen lone pair [116,117]. Thus, adding **1d** to a solution of **P3** caused no significant change in the porphyrin UV-Vis spectrum (Table 2, line 23). However, by taking advantage of the trends revealed for **1a**, we supposed that **P8** and **P9** could again be the preferred hosts in the case of **1d** as well. Although planar **P8** afforded a relatively small value of the association constant being around 450 M^{-1}, non-planar **P9** with its eight additional bromine atoms resulted in the considerable increase in K_a of up to (1.16 ± 0.07) × 10^4.

3.3. Circular Dichroism Spectra

Coordination of a chiral guest to a planar and achiral porphyrin host typically induces a notable CD signal in the region of the porphyrin Soret band and allows the guest's chirality to be sensed. This was the case for almost all the host–guest systems studied (Table 3; Figure 7, see also Supplementary Materials), with only two exceptions of the CD-silent complexes (*R*,*R*)-**1a**·**P7** and (*S*,*S*)-**1d**·**P9**. The CD spectra were measured at the end point of UV-Vis titration experiments with a high molar excess of the thiourea guests that corresponded to 87−99% conversion of unligated zinc porphyrin into the complex, as calculated by the values of the association constants. The (chir)optical outcome is clearly specific for a certain host–guest combination, with respect to both the amplitude and sign of observed Cotton effects (CE). Such variability is not unexpected in the view of the complex

origin of net CD signal [26,69,101,118–120]. Enantiomers of compound **1a** display CD signal in the far-UV region with λ_{max} of 253 nm and 308 nm and intensities of 15 $M^{-1}\cdot cm^{-1}$ and 28 $M^{-1}\cdot cm^{-1}$, respectively (see Figure S86 in the Supplementary Materials).

Table 3. CD data for the complexes of zinc porphyrins **P1–P9** with thioureas **1a–d** measured in CH_2Cl_2.

Entry	Complex	CE λ_{max}, nm ($\Delta\varepsilon$, $M^{-1}\cdot cm^{-1}$) [a]
1	(*R*,*R*)-**1a**·**P1**	439 (+3)
2	(*R*,*R*)-**1a**·**P2**	432 (−25)
3	(*R*,*R*)-**1a**·**P3**	429 (−25), 436 (+5) [b]
4	(*R*,*R*)-**1a**·**P4**	425 (−7), 432 (+11)
5	(*R*,*R*)-**1a**·**P5**	425 (−6), 434 (+12)
6	(*R*,*R*)-**1a**·**P6**	426 (−10), 432 (+12)
7	(*R*,*R*)-**1a**·**P7**	n.d.
8	(*R*,*R*)-**1a**·**P8**	426 (+8)
9	(*R*,*R*)-**1a**·**P9**	481 (+3)
10	(*R*,*R*)-**1b**·**P2**	430 (+10)
11	(*R*,*R*)-**1b**·**P3**	429 (+9) [b]
12	(*R*,*R*)-**1b**·**P5**	430 (+23)
13	(*R*,*R*)-**1b**·**P6**	429 (+20)
14	(*R*,*R*)-**1b**·**P7**	433 (+21)
15	(*R*,*R*)-**1c**·**P1**	433 (+12)
16	(*R*,*R*)-**1c**·**P2**	435 (+13)
17	(*R*,*R*)-**1c**·**P3**	430 (+15) [b]
18	(*R*,*R*)-**1c**·**P5**	431 (+23)
19	(*R*,*R*)-**1c**·**P6**	431 (+25)
20	(*R*,*R*)-**1c**·**P7**	433 (+22)
21	(*R*,*R*)-**1c**·**P8**	426 (+21)
22	(*S*,*S*)-**1d**·**P8**	423 (+7)
23	(*S*,*S*)-**1d**·**P9**	n.d.

[a] The noise level is up to ± 2.3 $M^{-1}\cdot cm^{-1}$. [b] The host–guest system has been previously described [60].

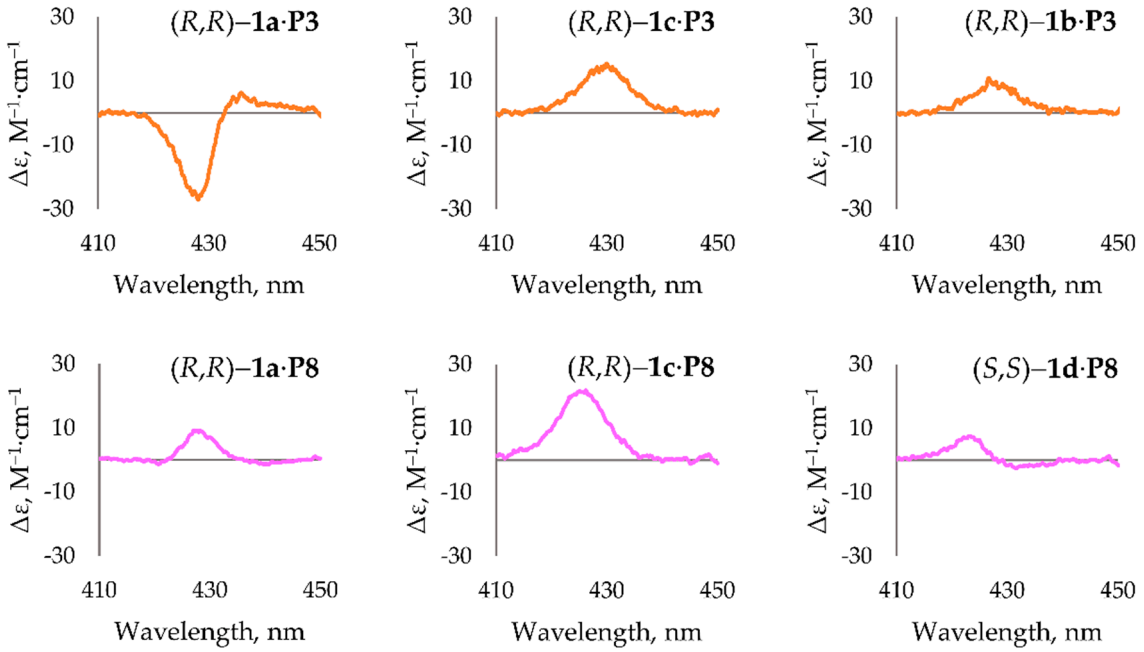

Figure 7. Representative experimental CD spectra obtained for the complexes of thioureas **1a–d** with zinc porphyrins **P3** and **P8** (CH_2Cl_2, 293 K). The complete CD spectral data for all studied host–guest pairs is provided in the Supplementary Materials.

Previously, we showed that conformational changes in **1a** produced different CD outcomes in the **1a**·**P3** complex [60]. The overall CD spectrum profile, consisting of a weak positive and relatively strong negative CEs (Figure 7; Table 3, line 3), was determined as a Boltzmann average of the separate conformer's inputs and perfectly matched the experimental spectrum. Analogously, it is reasonable to assume that the CD spectra observed for the sibling complexes simply reflect the differences in the respective conformational compositions, mostly determined by the guest molecules as components with a higher degree of conformational freedom. Indeed, despite the rather specific (chir)optical outcomes observed in these supramolecular complexes (Figure 7, Table 3), some generalizations can be tentatively outlined, supporting this hypothesis. In the series of complexes with structurally similar *p*-substituted ZnTPP hosts (**P2**–**P7**), the (chir)optical outcome is mostly determined by the guest, while the porphyrin host has a somewhat secondary impact. Thus, thioureas **1b** and **1c** are inclined to induce monosignate positive CEs (Figure 7, Table 3, lines 10–21). However, it can be noted that in the case of **1a**, the rise of electronegativity in the porphyrin binding site results in a positive monosignate signal to transform into a bisignate CD signal (see Figure S84 in the Supplementary Materials). Moreover, the complexes of **1a** with the most electronegative porphyrins of the selection **P2** and **P1** produce a monosignate negative CD signal only.

It is worth noting that the amplitudes of the induced CD signals do not correlate with the values of association constants, e.g., the complex (*R*,*R*)-**1c**·**P5** gives virtually the same maximal CE intensity (+23 $M^{-1}{\cdot}cm^{-1}$; line 18 in Table 3) as that of the complex (*R*,*R*)-**1c**·**P8** (+21 $M^{-1}{\cdot}cm^{-1}$; line 21 in Table 3) possessing an order of magnitude greater association constant (see Table 2, lines 18 and 22). While the maximum CE intensity was found to be $\pm$25 $M^{-1}{\cdot}cm^{-1}$, CD silent spectra were observed for (*R*,*R*)-**1a**·**P7** and (*S*,*S*)-**1d**·**P9**, apparently due to mutual compensation of the oppositely-signed CD signals of different host–guest conformers. Unfortunately, the strongly complexing porphyrins **P8** and **P9** produce rather modest CD responses for the analytes of major concern due to their toxicity (**1a** and **1d**). This implies that further structural modifications of these hosts are required for better sensing adaptation, to enhance the (chir)optical outcome and preserve high association constant values. Highly electron-deficient porphyrins **P8** and **P9** can be considered as good starting scaffolds for such modifications.

4. Conclusions

Given the toxic effect revealed for 3,5-bis(trifluoromethyl)phenyl)-substituted thioureas **1a** and **1d** (Takemoto's catalyst) in the *Vibrio fischeri* luminescence inhibition test, these conventional organocatalysts and similar compounds might pose an environmental pollution risk. Although additional ecotoxicology and biodegradation studies are required to clearly manifest their ecological impact, **1a** and **1d** can be considered as emerging chiral pollutants, for which a reliable instrumental detection method must be developed.

We have addressed this important environmental issue for the first time. Thus, the solution detection of **1a–d** and similar nitrogen-containing chiral pollutants could be based on supramolecular binding with suitable zinc porphyrin hosts in which the Zn$\cdots$N cation-dipole interaction is dominant, and the complex stability increases with the rising electron-withdrawing properties of the porphyrin host. As a first step in this direction, we have performed selective screening of several zinc porphyrins **P1**–**P9** with a gradual increase in the electron-withdrawing properties to identify the best sensory candidates in terms of the highest values of its association constants (in range from 10^2 to 10^5 M^{-1}) and (chir)optical response (from negative to positive CE). For the target analytes **1a** and **1d**, the electron-deficient and non-planar porphyrin **P9** was revealed as the strongest binder, which could be particularly suitable for further practical adaptations. Additional non-covalent interactions, such as weak π–π interactions provided by the aromatic groups or hydrogen bonding ensured by the thiourea moiety, might be present in the host–guest systems studied, and could be used to enhance the sensory sensitivity and selectivity. However, based on our study, we recommend using porphyrins **P2** and **P3** to detect of chiral pollutant **1a** due to

the strong and specific (chir)optical outcomes. To detect chiral pollutant **1d**, porphyrin **P8** gives the best (chir)optical response out of our current porphyrin library.

It was found that the (chir)optical outcome was specific for certain host–guest combinations, with respect to the amplitude, sign, and the number of observed CEs induced in the Soret band region with the maximal CE intensity of $\pm 25\ M^{-1} \cdot cm^{-1}$. For a better and clearly interpretable CD response, further structural modification of the parent hosts **P8** and **P9** is needed to attenuate the adverse effects caused by the guests' conformational flexibility. For this purpose, introducing additional binding point(s) specific to the thiourea functionalities could be one of the host's further developments. The design and investigation of the next generation of porphyrin hosts based on these principles, suitable for the effective detection of chiral pollutants in real-world environments, are currently in progress at our laboratory. A comprehensive analysis of CD induction phenomena in these systems, crucial for the sensor design, will be reported in due course.

Supplementary Materials: The following are available online at "https://www.mdpi.com/article/10.3390/chemosensors9100278/s1, spectroscopic UV-Vis titrations' data (raw data, curve fittings and residuals analysis); UV-Vis spectra; CD spectra; NSD distortion analysis for the porphyrin core in **1b**·**P5**; determination of dimerization constants for **1a** and **1c** by ^{1}H NMR spectroscopy; computational details, including Cartesian coordinates".

Author Contributions: Conceptualization and idea of the research, D.K. and V.B.; synthesis of compounds, N.K., M.H. and M.K.; spectroscopic host–guest binding studies, N.K. and M.H.; computational studies, I.O.; X-ray studies, K.-N.T. and K.R.; NMR studies, J.A. and M.H.; toxicity studies, M.S. and A.K.; formal analysis, N.K., M.H., K.-N.T., M.S. and D.K.; data analysis, T.B. and I.O.; writing—original draft preparation, D.K.; writing—review and editing, D.K., V.B., K.-N.T., N.K., M.S., A.K., M.O.S., N.K., M.H., I.O. and R.A.; supervision, D.K., K.R., A.K., M.O.S. and R.A.; project administration, R.A.; funding acquisition, I.O., M.O.S., V.B. and R.A. All authors have read and agreed to the published version of the manuscript.

Funding: This work was supported by the Estonian Research Council grant PUTJD749 (for I.O.) PRG399, (for N.K., R.A., V.B.), PSG400 (for J.A), PRG749 (for M.S.), European Regional Development Fund grants NAMUR+ 2014-2020.4.01.16-0123 (for M.S. and A.K) and TK134 (for A.K., J.A.) and the European Union's H2020-FETOPEN grant 828779 (INITIO) (for N.K., K.-N.T., K.R., M.K., M.O.S., D.K., R.A., V.B.). M.H. is grateful to the Dora Plus program for financial support of his research stay at Tallinn University of Technology.

Institutional Review Board Statement: Not applicable.

Informed Consent Statement: Not applicable.

Data Availability Statement: The data presented in this study are available in the article and supplementary materials.

Acknowledgments: We are grateful to Tatsiana Dalidovich (TalTech) for preparation of zinc porphyrins **P1** and **P8** from the corresponding free base porphyrins, and Jagadeesh Varma Nallaparaju (TalTech) for his assistance with the preparation of thioureas **1a–c**. Tatsiana Dalidovich and Jevgenija Martõnova (TalTech) are acknowledged for their generous assistance with samples preparation for ^{1}H NMR and toxicity studies. Computational studies were performed on the HPC cluster at Tallinn University of Technology (TalTech), which is part of the ETAIS project and partly on at Computational Chemistry laboratory at TalTech. I.O. acknowledges Toomas Tamm for his kind help.

Conflicts of Interest: The authors declare no conflict of interest.

References

1. Jeschke, P. Current status of chirality in agrochemicals. *Pest. Manag. Sci.* **2018**, *74*, 2389–2404. [CrossRef]
2. Blaser, H.-U. Chirality and its implications for the pharmaceutical industry. *Rend. Lincei* **2013**, *24*, 213–216. [CrossRef]
3. Agranat, I.; Wainschtein, S.R.; Zusman, E.Z. The predicated demise of racemic new molecular entities is an exaggeration. *Nat. Rev. Drug Discov.* **2012**, *11*, 972–973. [CrossRef]
4. Kasprzyk-Hordern, B. Pharmacologically active compounds in the environment and their chirality. *Chem. Soc. Rev.* **2010**, *39*, 4466–4503. [CrossRef] [PubMed]

5. Sanganyado, E.; Lu, Z.; Fu, Q.; Schlenk, D.; Gan, J. Chiral pharmaceuticals: A review on their environmental occurrence and fate processes. *Water Res.* **2017**, *124*, 527–542. [CrossRef] [PubMed]
6. Kümmerer, K. *Pharmaceuticals in the Environment*; Springer: Berlin/Heidelberg, Germany, 2004.
7. Richter, E.; Wick, A.; Ternes, T.A.; Coors, A. Ecotoxicity of climbazole, a fungicide contained in antidandruff shampoo. *Environ. Toxicol. Chem.* **2013**, *32*, 2816–2825. [CrossRef] [PubMed]
8. Maia, A.S.; Ribeiro, A.R.; Castro, P.M.L.; Tiritan, M.E. Chiral analysis of pesticides and drugs of environmental concern: Biodegradation and enantiomeric fraction. *Symmetry* **2017**, *9*, 196. [CrossRef]
9. Ulrich, E.M.; Morrison, C.N.; Goldsmith, M.R.; Foreman, W.T. Chiral pesticides: Identification, description, and environmental implications. *Rev. Environ. Contam. Toxicol.* **2012**, *217*, 1–74.
10. You, L.; Zha, D.; Anslyn, E.V. Recent advances in supramolecular analytical chemistry using optical sensing. *Chem. Rev.* **2015**, *115*, 7840–7892. [CrossRef]
11. Mako, T.L.; Racicot, J.M.; Levine, M. Supramolecular luminescent sensors. *Chem. Rev.* **2019**, *119*, 322–477. [CrossRef]
12. Minami, T. Design of Supramolecular sensors and their applications to optical chips and organic devices. *Bull. Chem. Soc. Jpn.* **2020**, *94*, 24–33. [CrossRef]
13. Paolesse, R.; Nardis, S.; Monti, D.; Stefanelli, M.; Di Natale, C. Porphyrinoids for chemical sensor applications. *Chem. Rev.* **2017**, *117*, 2517–2583. [CrossRef]
14. Hembury, G.A.; Borovkov, V.V.; Inoue, Y. Chirality-sensing supramolecular systems. *Chem. Rev.* **2008**, *108*, 1–73. [CrossRef] [PubMed]
15. Borovkov, V.V.; Lintuluoto, J.M.; Inoue, Y. Supramolecular chirogenesis in bis (zinc porphyrin): An absolute configuration probe highly sensitive to guest structure. *Org. Lett.* **2000**, *2*, 1565–1568. [CrossRef] [PubMed]
16. Lintuluoto, J.M.; Borovkov, V.V.; Inoue, Y. Direct determination of absolute configuration of monoalcohols by bis (magnesium porphyrin). *J. Am. Chem. Soc.* **2002**, *124*, 13676–13677. [CrossRef] [PubMed]
17. Takeda, S.; Hayashi, S.; Noji, M.; Takanami, T. Chiroptical protocol for the absolute configurational assignment of Alkyl-substituted epoxides using bis (zinc porphyrin) as a CD-sensitive bidentate host. *J. Org. Chem.* **2019**, *84*, 645–652. [CrossRef]
18. Chmielewski, P.J.; Siczek, M.; Stępień, M. Bis (N-Confused Porphyrin) as a semirigid receptor with a chirality memory: A two-way host enantiomerization through point-to-axial chirality transfer. *Chem.-A Eur. J.* **2015**, *21*, 2547–2559. [CrossRef] [PubMed]
19. Gholami, H.; Chakraborty, D.; Zhang, J.; Borhan, B. Absolute stereochemical determination of organic molecules through induction of helicity in host–guest complexes. *Acc. Chem. Res.* **2021**, *54*, 654–667. [CrossRef]
20. Lamberth, C. Heterocyclic chemistry in crop protection. *Pest Manag. Sci.* **2013**, *69*, 1106–1114. [CrossRef]
21. Ertl, P.; Altmann, E.; McKenna, J.M. The most common functional groups in bioactive molecules and how their popularity has evolved over time. *J. Med. Chem.* **2020**, *63*, 8408–8418. [CrossRef]
22. Kerru, N.; Gummidi, L.; Maddila, S.; Gangu, K.K.; Jonnalagadda, S.B. A review on recent advances in nitrogen-containing molecules and their biological applications. *Molecules* **2020**, *25*, 1909. [CrossRef] [PubMed]
23. Borovkov, V.V.; Lintuluoto, J.M.; Sugeta, H.; Fujiki, M.; Arakawa, R.; Inoue, Y. Supramolecular chirogenesis in zinc porphyrins: Equilibria, binding properties, and thermodynamics. *J. Am. Chem. Soc.* **2002**, *124*, 2993–3006. [CrossRef]
24. Ito, S.; Hiroto, S.; Ousaka, N.; Yashima, E.; Shinokubo, H. Control of conformation and chirality of nonplanar π-conjugated diporphyrins using substituents and axial ligands. *Chem.-Asian J.* **2016**, *11*, 936–942. [CrossRef] [PubMed]
25. Olsson, S.; Schäfer, C.; Blom, M.; Gogoll, A. Exciton-coupled circular dichroism characterization of monotopically binding guests in host−guest complexes with a bis (zinc porphyrin) tweezer. *Chempluschem* **2018**, *83*, 1169–1178. [CrossRef]
26. Mizutani, T.; Ema, T.; Yoshida, T.; Renne, T.; Ogoshi, H. Mechanism of induced circular dichroism of amino acid ester-porphyrin supramolecular systems. Implications to the origin of the circular dichroism of hemoprotein. *Inorg. Chem.* **1994**, *33*, 3558–3566. [CrossRef]
27. Mizutani, T.; Kurahashi, T.; Murakami, T.; Matsumi, N.; Ogoshi, H. Molecular recognition of carbohydrates by zinc porphyrins: Lewis acid/lewis base combinations as a dominant factor for their selectivity. *J. Am. Chem. Soc.* **1997**, *119*, 8991–9001. [CrossRef]
28. Imai, H.; Munakata, H.; Uemori, Y.; Sakura, N. Chiral recognition of amino acids and dipeptides by a water-soluble zinc porphyrin. *Inorg. Chem.* **2004**, *43*, 1211–1213. [CrossRef]
29. Gomollón-Bel, F. Ten chemical innovations that will change our world: IUPAC identifies emerging technologies in Chemistry with potential to make our planet more sustainable. *Chem. Int.* **2019**, *41*, 12–17. [CrossRef]
30. Schreiner, P.R.; Wittkopp, A. H-bonding additives act like lewis acid catalysts. *Org. Lett.* **2002**, *4*, 217–220. [CrossRef]
31. Sigman, M.S.; Jacobsen, E.N. Schiff base catalysts for the asymmetric strecker reaction identified and optimized from parallel synthetic libraries. *J. Am. Chem. Soc.* **1998**, *120*, 4901–4902. [CrossRef]
32. Okino, T.; Hoashi, Y.; Takemoto, Y. Enantioselective Michael reaction of malonates to nitroolefins catalyzed by bifunctional organocatalysts. *J. Am. Chem. Soc.* **2003**, *125*, 12672–12673. [CrossRef]
33. Serdyuk, O.V.; Heckel, C.M.; Tsogoeva, S.B. Bifunctional primary amine-thioureas in asymmetric organocatalysis. *Org. Biomol. Chem.* **2013**, *11*, 7051–7071. [CrossRef]
34. Steppeler, F.; Iwan, D.; Wojaczyńska, E.; Wojaczyński, J. Chiral thioureas—preparation and significance in asymmetric synthesis and medicinal chemistry. *Molecules* **2020**, *25*, 401. [CrossRef]
35. Takemoto, Y. Recognition and activation by ureas and thioureas: Stereoselective reactions using ureas and thioureas as hydrogen-bonding donors. *Org. Biomol. Chem.* **2005**, *3*, 4299–4306. [CrossRef]

36. Limnios, D.; Kokotos, C.G. Chapter 19 ureas and thioureas as asymmetric organocatalysts. In *Sustainable Catalysis: Without Metals or Other Endangered Elements, Part 2*; The Royal Society of Chemistry: London, UK, 2015; pp. 196–255.
37. Pratt, R.C.; Lohmeijer, B.G.G.; Long, D.A.; Lundberg, P.N.P.; Dove, A.P.; Li, H.; Wade, C.G.; Waymouth, R.M.; Hedrick, J.L. Exploration, optimization, and application of supramolecular thiourea−amine catalysts for the synthesis of lactide (Co) polymers. *Macromolecules* **2006**, *39*, 7863–7871. [CrossRef]
38. Kamber, N.E.; Jeong, W.; Waymouth, R.M.; Pratt, R.C.; Lohmeijer, B.G.G.; Hedrick, J.L. Organocatalytic ring-opening polymerization. *Chem. Rev.* **2007**, *107*, 5813–5840. [CrossRef]
39. Orhan, B.; Tschan, M.J.-L.; Wirotius, A.-L.; Dove, A.P.; Coulembier, O.; Taton, D. Isoselective ring-opening polymerization of rac-lactide from Chiral Takemoto's organocatalysts: Elucidation of stereocontrol. *ACS Macro Lett.* **2018**, *7*, 1413–1419. [CrossRef]
40. SciFinder database. Available online: https://scifinder.cas.org/ (accessed on 28 April 2021).
41. Egorova, K.S.; Ananikov, V.P. Which metals are green for catalysis? Comparison of the toxicities of Ni, Cu, Fe, Pd, Pt, Rh, and au salts. *Angew. Chem. Int. Ed.* **2016**, *55*, 12150–12162. [CrossRef] [PubMed]
42. Egorova, K.S.; Ananikov, V.P. Toxicity of metal compounds: Knowledge and myths. *Organometallics* **2017**, *36*, 4071–4090. [CrossRef]
43. Hayes, T. *Green Organocatalysis: An (eco)-Toxicity and Biodegradation Study of Organocatalysts*; Dublin City University: Dublin, Ireland, 2012.
44. Nachtergael, A.; Coulembier, O.; Dubois, P.; Helvenstein, M.; Duez, P.; Blankert, B.; Mespouille, L. Organocatalysis paradigm revisited: Are metal-free catalysts really harmless? *Biomacromolecules* **2015**, *16*, 507–514. [CrossRef] [PubMed]
45. Mortimer, M.; Kasemets, K.; Heinlaan, M.; Kurvet, I.; Kahru, A. High throughput kinetic Vibrio fischeri bioluminescence inhibition assay for study of toxic effects of nanoparticles. *Toxicol. Vitr.* **2008**, *22*, 1412–1417. [CrossRef]
46. Dudziński, K.; Pakulska, A.M.; Kwiatkowski, P. An efficient organocatalytic method for highly enantioselective michael addition of malonates to enones catalyzed by readily accessible primary amine-thiourea. *Org. Lett.* **2012**, *14*, 4222–4225. [CrossRef] [PubMed]
47. Zhang, X.-J.; Liu, S.-P.; Lao, J.-H.; Du, G.-J.; Yan, M.; Chan, A.S. Asymmetric conjugate addition of carbonyl compounds to nitroalkenes catalyzed by chiral bifunctional thioureas. *Tetrahedron Asymmetry* **2009**, *20*, 1451–1458. [CrossRef]
48. Borovkov, V.V.; Lintuluoto, J.M.; Inoue, Y. Synthesis of Zn-, Mn-, and Fe-containing mono- and heterometallated ethanediyl-bridged porphyrin dimers. *Helv. Chim. Acta* **1999**, *82*, 919–934. [CrossRef]
49. Kojima, T.; Nakanishi, T.; Honda, T.; Harada, R.; Shiro, M.; Fukuzumi, S. Impact of distortion of porphyrins on axial coordination in (Porphyrinato) zinc (II) complexes with aminopyridines as axial ligands. *Eur. J. Inorg. Chem.* **2009**, *2009*, 727–734. [CrossRef]
50. Mandon, D.; Ochenbein, P.; Fischer, J.; Weiss, R.; Jayaraj, K.; Austin, R.N.; Gold, A.; White, P.S.; Brigaud, O. beta.-Halogenated-pyrrole porphyrins. Molecular structures of 2,3,7,8,12,13,17,18-octabromo-5,10,15,20-tetramesitylporphyrin, nickel (II) 2,3,7,8,12,13,17,18-octabromo-5,10,15,20-tetramesitylporphyrin, and nickel (II) 2,3,7,8,12,13,17,18-octabromo-5,10,15. *Inorg. Chem.* **1992**, *31*, 2044–2049. [CrossRef]
51. Online Tools for Supramolecular Chemistry Research and Analysis. Available online: http://supramolecular.org/ (accessed on 15 May 2021).
52. Brynn Hibbert, D.; Thordarson, P. The death of the Job plot, transparency, open science and online tools, uncertainty estimation methods and other developments in supramolecular chemistry data analysis. *Chem. Commun.* **2016**, *52*, 12792–12805. [CrossRef]
53. Hirose, K. A practical guide for the determination of binding constants. *J. Incl. Phenom. Macrocycl. Chem.* **2001**, *39*, 193–209. [CrossRef]
54. Lehnherr, D.; Ford, D.D.; Bendelsmith, A.J.; Rose Kennedy, C.; Jacobsen, E.N. Conformational control of chiral amido-thiourea catalysts enables improved activity and enantioselectivity. *Org. Lett.* **2016**, *18*, 3214–3217. [CrossRef]
55. Nogales, D.F.; Ma, J.-S.; Lightner, D.A. Self-association of dipyrrinones observed by 2d-noe nmr and dimerization constants calculated from 1h-nmr chemical shifts. *Tetrahedron* **1993**, *49*, 2361–2372. [CrossRef]
56. *Rigaku Oxford Diffraction, CrysAlisPro Software System*; Version 38.46; Rigaku Corporation Oxford: Oxford, UK, 2017.
57. Sheldrick, G.M. A short history of *SHELX*. *Acta Crystallogr. Sect. A* **2008**, *64*, 112–122. [CrossRef]
58. Sheldrick, G.M. *SHELXL13. Program Package for Crystal Structure Determination from Single Crystal Diffraction Data*; University of Göttingen: Göttingen, Germany, 2013.
59. Sheldrick, G.M. Crystal structure refinement with *SHELXL*. *Acta Crystallogr. Sect. C* **2015**, *71*, 3–8. [CrossRef]
60. Konrad, N.; Meniailava, D.; Osadchuk, I.; Adamson, J.; Hasan, M.; Clot, E.; Aav, R.; Borovkov, V.; Kananovich, D. Supramolecular chirogenesis in zinc porphyrins: Complexation with enantiopure thiourea derivatives, binding studies and chirality transfer mechanism. *J. Porphyr. Phthalocyanines* **2019**, *24*, 840–849. [CrossRef]
61. Eichkorn, K.; Treutler, O.; Öhm, H.; Häser, M.; Ahlrichs, R. Auxiliary basis sets to approximate Coulomb potentials. *Chem. Phys. Lett.* **1995**, *240*, 283–290. [CrossRef]
62. Eichkorn, K.; Weigend, F.; Treutler, O.; Ahlrichs, R. Auxiliary basis sets for main row atoms and transition metals and their use to approximate Coulomb potentials. *Theor. Chem. Acc.* **1997**, *97*, 119–124. [CrossRef]
63. Sierka, M.; Hogekamp, A.; Ahlrichs, R. Fast evaluation of the Coulomb potential for electron densities using multipole accelerated resolution of identity approximation. *J. Chem. Phys.* **2003**, *118*, 9136–9148. [CrossRef]
64. Becke, A.D. Density-functional exchange-energy approximation with correct asymptotic behavior. *Phys. Rev. A* **1988**, *38*, 3098–3100. [CrossRef]

65. Perdew, J.P. Density-functional approximation for the correlation energy of the inhomogeneous electron gas. *Phys. Rev. B* **1986**, *33*, 8822–8824. [CrossRef] [PubMed]
66. Grimme, S.; Antony, J.; Ehrlich, S.; Krieg, H. A consistent and accurate ab initio parametrization of density functional dispersion correction (DFT-D) for the 94 elements H-Pu. *J. Chem. Phys.* **2010**, *132*, 154104. [CrossRef]
67. Schäfer, A.; Horn, H.; Ahlrichs, R. Fully optimized contracted Gaussian basis sets for atoms Li to Kr. *J. Chem. Phys.* **1992**, *97*, 2571–2577. [CrossRef]
68. TURBOMOLE V7.0 2015, a Development of University of Karlsruhe and Forschungszentrum Karlsruhe GmbH, 1089–2007, TURBOMOLE GmbH, Since 2007. Available online: http://www.turbomole.com (accessed on 28 April 2021).
69. Osadchuk, I.; Borovkov, V.; Aav, R.; Clot, E. Benchmarking computational methods and influence of guest conformation on chirogenesis in zinc porphyrin complexes. *Phys. Chem. Chem. Phys.* **2020**, *22*, 11025–11037. [CrossRef]
70. Martynov, A.G.; Mack, J.; May, A.K.; Nyokong, T.; Gorbunova, Y.G.; Tsivadze, A.Y. Methodological survey of simplified TD-DFT methods for fast and accurate interpretation of UV-Vis–NIR spectra of phthalocyanines. *ACS Omega* **2019**, *4*, 7265–7284. [CrossRef]
71. Schmidt, N.; Fink, R.; Hieringer, W. Assignment of near-edge x-ray absorption fine structure spectra of metalloporphyrins by means of time-dependent density-functional calculations. *J. Chem. Phys.* **2010**, *133*, 054703. [CrossRef]
72. Weigend, F. Accurate Coulomb-fitting basis sets for H to Rn. *Phys. Chem. Chem. Phys.* **2006**, *8*, 1057–1065. [CrossRef]
73. Andzelm, J.; Kölmel, C.; Klamt, A. Incorporation of solvent effects into density functional calculations of molecular energies and geometries. *J. Chem. Phys.* **1995**, *103*, 9312–9320. [CrossRef]
74. Bader, R.F.W. Atoms in molecules. *Acc. Chem. Res.* **1985**, *18*, 9–15. [CrossRef]
75. Bader, R.F.W. A quantum theory of molecular structure and its applications. *Chem. Rev.* **1991**, *91*, 893–928. [CrossRef]
76. Keith, T.A. *AIMAll*; Version 19.10.12; Gristmill Software: Overland Park KS, USA, 2019. Available online: aim.tkgristmill.com (accessed on 28 April 2021).
77. Reed, A.E.; Curtiss, L.A.; Weinhold, F. Intermolecular interactions from a natural bond orbital, donor-acceptor viewpoint. *Chem. Rev.* **1988**, *88*, 899–926. [CrossRef]
78. Weinhold, F. Nature of H-bonding in clusters, liquids, and enzymes: An ab initio, natural bond orbital perspective. *J. Mol. Struct. THEOCHEM* **1997**, *398–399*, 181–197. [CrossRef]
79. Glendening, E.D.; Reed, A.E.; Carpenter, J.E.; Weinhold, F. *NBO*, Version 3.1. Available online: https://gaussian.com/citation/ (accessed on 28 April 2021).
80. Frisch, M.J.; Trucks, G.W.; Schlegel, H.B.; Scuseria, G.E.; Robb, M.A.; Cheeseman, J.R.; Scalmani, G.; Barone, V.; Petersson, G.A.; Nakatsuji, H.; et al. *Gaussian 16, Revision B.01*; Gaussian, Inc.: Wallingford, CT, USA, 2016. Available online: https://gaussian.com/citation_b01/ (accessed on 28 April 2021).
81. Chai, J.-D.; Head-Gordon, M. Long-range corrected hybrid density functionals with damped atom–atom dispersion corrections. *Phys. Chem. Chem. Phys.* **2008**, *10*, 6615–6620. [CrossRef]
82. Dunning, T.H. Gaussian basis sets for use in correlated molecular calculations. I. The atoms boron through neon and hydrogen. *J. Chem. Phys.* **1989**, *90*, 1007–1023. [CrossRef]
83. Kendall, R.A.; Dunning, T.H.; Harrison, R.J. Electron affinities of the first-row atoms revisited. Systematic basis sets and wave functions. *J. Chem. Phys.* **1992**, *96*, 6796–6806. [CrossRef]
84. Woon, D.E.; Dunning, T.H. Gaussian basis sets for use in correlated molecular calculations. III. The atoms aluminum through argon. *J. Chem. Phys.* **1993**, *98*, 1358–1371. [CrossRef]
85. Marenich, A.V.; Cramer, C.J.; Truhlar, D.G. Universal solvation model based on solute electron density and on a continuum model of the solvent defined by the bulk dielectric constant and atomic surface tensions. *J. Phys. Chem. B* **2009**, *113*, 6378–6396. [CrossRef] [PubMed]
86. Dennington, R.; Keith, T.A.; Millam, J.M. *GaussView*, Version 6; Semichem Inc.: Shawnee Mission, KS, USA. Available online: https://gaussian.com/citation/ (accessed on 28 April 2021).
87. ISO. *Water Quality—Kinetic Determination of the Inhibitory Effects of Sediment, Other Solids and Coloured Samples on the Light Emission of Vibrio fischeri (Kinetic Luminescent Bacteria Test)*; ISO 21338: Geneva, Switzerland, 2010.
88. Vindimian, E. REGTOX: Macro ExcelTM pour dose-réponse. Available online: http://www.normalesup.org/~{}vindimian/en_index.html (accessed on 8 December 2020).
89. Kahru, A. In vitro toxicity testing using marine luminescent bacteria (*Photobacterium* phosphoreum): The Biotox^{TM} test. *Altern. Lab. Anim.* **1993**, *21*, 210–215. [CrossRef]
90. Kusumahastuti, D.K.A.; Sihtmäe, M.; Kapitanov, I.V.; Karpichev, Y.; Gathergood, N.; Kahru, A. Toxicity profiling of 24 l-phenylalanine derived ionic liquids based on pyridinium, imidazolium and cholinium cations and varying alkyl chains using rapid screening Vibrio fischeri bioassay. *Ecotoxicol. Environ. Saf.* **2019**, *172*, 556–565. [CrossRef] [PubMed]
91. Kahru, A.; Põllumaa, L. Environmental hazard of the waste streams of Estonian oil shale industry: An ecotoxicological review. *Oil Shale* **2006**, *23*, 53–93.
92. Aruoja, V.; Sihtmäe, M.; Dubourguier, H.-C.; Kahru, A. Toxicity of 58 substituted anilines and phenols to algae Pseudokirchneriella subcapitata and bacteria Vibrio fischeri: Comparison with published data and QSARs. *Chemosphere* **2011**, *84*, 1310–1320. [CrossRef]
93. Kurvet, I.; Ivask, A.; Bondarenko, O.; Sihtmäe, M.; Kahru, A. LuxCDABE—Transformed constitutively bioluminescent escherichia coli for toxicity screening: Comparison with naturally luminous vibrio fischeri. *Sensors* **2011**, *11*, 7865–7878. [CrossRef]

94. Wilhelm, E.A.; Jesse, C.R.; Nogueira, C.W.; Savegnago, L. Introduction of trifluoromethyl group into diphenyl diselenide molecule alters its toxicity and protective effect against damage induced by 2-nitropropane in rats. *Exp. Toxicol. Pathol.* **2009**, *61*, 197–203. [CrossRef]
95. Li, X.; Deng, H.; Zhang, B.; Li, J.; Zhang, L.; Luo, S.; Cheng, J.-P. Physical organic study of structure–activity–enantioselectivity relationships in asymmetric bifunctional thiourea catalysis: Hints for the design of new organocatalysts. *Chem.-A Eur. J.* **2010**, *16*, 450–455. [CrossRef]
96. Lippert, K.M.; Hof, K.; Gerbig, D.; Ley, D.; Hausmann, H.; Guenther, S.; Schreiner, P.R. Hydrogen-bonding thiourea organocatalysts: The privileged 3,5-bis (trifluoromethyl)phenyl group. *Eur. J. Org. Chem.* **2012**, *2012*, 5919–5927. [CrossRef]
97. Jakab, G.; Tancon, C.; Zhang, Z.; Lippert, K.M.; Schreiner, P.R. (Thio) urea organocatalyst equilibrium acidities in DMSO. *Org. Lett.* **2012**, *14*, 1724–1727. [CrossRef]
98. Kreienborg, N.M.; Merten, C. How do substrates bind to a bifunctional thiourea catalyst? A vibrational CD study on carboxylic acid binding. *Chem.-A Eur. J.* **2018**, *24*, 17948–17954. [CrossRef]
99. Martinez, C.R.; Iverson, B.L. Rethinking the term "pi-stacking". *Chem. Sci.* **2012**, *3*, 2191–2201. [CrossRef]
100. Jentzen, W.; Song, X.-Z.; Shelnutt, J.A. Structural characterization of synthetic and protein-bound porphyrins in terms of the lowest-frequency normal coordinates of the macrocycle. *J. Phys. Chem. B* **1997**, *101*, 1684–1699. [CrossRef]
101. Kingsbury, C.J.; Senge, M.O. The shape of porphyrins. *Coord. Chem. Rev.* **2021**, *431*, 213760. [CrossRef]
102. NSD On-line Tool. Available online: https://www.kingsbury.id.au/nsd (accessed on 28 April 2021).
103. Király, P.; Soós, T.; Varga, S.; Vakulya, B.; Tárkányi, G. Self-association promoted conformational transition of (3R,4S,8R,9R)-9-[(3,5-bis (trifluoromethyl) phenyl))-thiourea] (9-deoxy)-epi-cinchonine. *Magn. Reson. Chem.* **2010**, *48*, 13–19. [CrossRef]
104. Obrzud, M.; Rospenk, M.; Koll, A. Structure of aggregates of dialkyl urea derivatives in solutions. *J. Phys. Chem. B* **2010**, *114*, 15905–15912. [CrossRef]
105. Obrzud, M.; Rospenk, M.; Koll, A. Self-aggregation mechanisms of N-alkyl derivatives of urea and thiourea. *Phys. Chem. Chem. Phys.* **2014**, *16*, 3209–3219. [CrossRef]
106. Jang, H.B.; Rho, H.S.; Oh, J.S.; Nam, E.H.; Park, S.E.; Bae, H.Y.; Song, C.E. DOSY NMR for monitoring self aggregation of bifunctional organocatalysts: Increasing enantioselectivity with decreasing catalyst concentration. *Org. Biomol. Chem.* **2010**, *8*, 3918–3922. [CrossRef]
107. Hansch, C.; Leo, A.; Taft, R.W. A survey of Hammett substituent constants and resonance and field parameters. *Chem. Rev.* **1991**, *91*, 165–195. [CrossRef]
108. Majerz, I.; Dziembowska, T. Aromaticity and through-space interaction between aromatic rings in [2.2] paracyclophanes. *J. Phys. Chem. A* **2016**, *120*, 8138–8147. [CrossRef]
109. Majerz, I.; Dziembowska, T. Substituent effect on inter-ring interaction in paracyclophanes. *Mol. Divers.* **2020**, *24*, 11–20. [CrossRef]
110. Caramori, G.F.; Galembeck, S.E. Computational study about through-bond and through-space interactions in [2.2] cyclophanes. *J. Phys. Chem. A* **2007**, *111*, 1705–1712. [CrossRef] [PubMed]
111. Sinnokrot, M.O.; Sherrill, C.D. Substituent effects in $\pi-\pi$ interactions: Sandwich and T-shaped configurations. *J. Am. Chem. Soc.* **2004**, *126*, 7690–7697. [CrossRef] [PubMed]
112. Hayashi, S.; Sugibayashi, Y.; Nakanishi, W. Quantum chemical calculations with the AIM approach applied to the π-interactions between hydrogen chalcogenides and naphthalene. *RSC Adv.* **2016**, *6*, 49651–49660. [CrossRef]
113. Roucan, M.; Kielmann, M.; Connon, S.J.; Bernhard, S.S.R.; Senge, M.O. Conformational control of nonplanar free base porphyrins: Towards bifunctional catalysts of tunable basicity. *Chem. Commun.* **2017**, *54*, 26–29. [CrossRef] [PubMed]
114. Marsh, R.E.; Schaefer, W.P.; Hodge, J.A.; Hughes, M.E.; Gray, H.B.; Lyons, J.E.; Ellis Jnr, P.E. A highly solvated zinc (II) tetrakis (pentafluorophenyl)-β-octabromoporphyrin. *Acta Cryst.* **1993**, *C49*, 1339–1342. [CrossRef]
115. Kielmann, M.; Senge, M.O. Molecular engineering of free-base porphyrins as ligands—The N−H···X binding motif in tetrapyrroles. *Angew. Chemie Int. Ed.* **2019**, *58*, 418–441. [CrossRef]
116. Andreev, V.P.; Sobolev, P.S.; Zaitsev, D.O.; Tafeenko, V.A. Complex formation between zinc (II) tetraphenylporphyrinate and alkylamines. *Russ. J. Gen. Chem.* **2014**, *84*, 320–325. [CrossRef]
117. Andreev, V.P.; Sobolev, P.S.; Zaitsev, D.O.; Remizova, L.A.; Tafeenko, V.A. Coordination of secondary and tertiary amines to zinc tetraphenylporphyrin. *Russ. J. Gen. Chem.* **2014**, *84*, 1979–1988. [CrossRef]
118. Osadchuk, I.; Aav, R.; Borovkov, V.; Clot, E. Chirogenesis in zinc porphyrins: Theoretical evaluation of electronic transitions, controlling structural factors, and axial ligation. *ChemPhysChem* **2021**, *22*, 1817–1833. [CrossRef]
119. Kiefl, C.; Sreerama, N.; Haddad, R.; Sun, L.; Jentzen, W.; Lu, Y.; Qiu, Y.; Shelnutt, J.A.; Woody, R.W. Heme distortions in sperm-whale carbonmonoxy myoglobin: Correlations between rotational strengths and heme distortions in MD-generated structures. *J. Am. Chem. Soc.* **2002**, *124*, 3385–3394. [CrossRef]
120. Osadchuk, I.; Konrad, N.; Truong, K.-N.; Rissanen, K.; Clot, E.; Aav, R.; Kananovich, D.; Borovkov, V. Supramolecular chirogenesis in bis-porphyrin: Crystallographic structure and cd spectra for a complex with a chiral guanidine derivative. *Symmetry* **2021**, *13*, 275. [CrossRef]